Milan Research Centre for
Industrial and Applied Mathematics

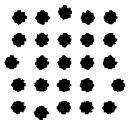

miriam

Mathematical Modelling & Computing in Biology and Medicine

5th ESMTB Conference 2002

Editor: V. Capasso

Editor

Vincenzo CAPASSO
MIRIAM - Milan Research Centre for
Industrial and Applied Mathematics
and
Department of Mathematics
University of Milano
Via C. Saldini, 50
20133 MILANO, Italy
E-mail: vincenzo.capasso@mat.unimi.it

ISBN 88-7488-055-3

PROGETTO LEONARDO

è una realizzazione
SOCIETÀ EDITRICE ESCULAPIO
40131 Bologna (Italy) - via U. Terracini 30 - Tel 051-63.40.343 - Fax 051-63.41.136

A Novel Mechanism for Mesenchymal Condensation during Limb Chondrogenesis in vitro

Wei Zeng[1], Gilberto L. Thomas[2,3], Stuart A. Newman[4], and James A. Glazier[1]

[1] Department of Physics and Biocomplexity Institute, Swain Hall West 159, 727 East 3rd Street, Indiana University, Bloomington, IN 47405-7105, USA
[2] Department of Physics and Interdisciplinary Center for the Study of Biocomplexity, University of Notre Dame, Notre Dame, IN 46556-5670, USA
[3] Instituto de Física, UFRGS, C. P. 15051, 91501-970 Porto Alegre, RS, Brazil
[4] Department of Cell Biology and Anatomy, New York Medical College, Valhalla, NY 10595, USA

Abstract. Mesenchymal condensation is a critical step in much early morphogenesis. We propose a stochastic model to explain cell clustering during condensation in limb bud cell cultures, based on local cell-cell adhesion and cell-extracellular matrix (ECM) interactions and implement a two-dimensional (2D) cellular Potts Model (CPM) simulation. The simulation reproduces some of the phenomenology of *in vitro* chick limb chondrogenic mesenchymal condensation at the local level, as well as aspects of the global distribution of condensations. In particular, our model provides an account of dispersed patterns of condensations without invoking Turing-type reaction-diffusion mechanisms, chemotaxis, or other mechanisms that require long-range cell signaling and movement. We discuss limitations and possible applicability of the model to three-dimensional chondrogenesis in the intact limb.

1 Introduction

In developing connective tissues, mesenchymal cells are initially dispersed in a hydrated ECM. In a crucial, common step in the formation of structures like skeletal elements, feather germs, blood vessels, or epithelial kidney tubules, these cells transiently reorganize into compact clusters through mesenchymal condensation.

The vertebrate limb develops from masses of mesodermally-derived mesenchymal tissue that emerge from the body wall. A pattern of mesenchymal condensation develops into an array of cartilage nodules and rods, which bone later replaces [1]. With regard to the formation of individual condensations, experiments support mechanisms involving generation of local adhesive differentials based on deposition of new extracellular matrix and production of cell-surface adhesion molecules, rather than mechanisms involving traction, chemotaxis or local loss of matrix [2–5]. In the quasi-2D 'micromass culture' (experimental method in the appendix) the series of developmental steps qualitatively resembles differentiation (chondrogenesis) *in vivo*: The

separated mesenchymal cells condense focally to form larger area contacts with one another than do the surrounding noncondensing cells. Finally, cells differentiate at the sites of condensation.

Accumulation of the adhesive extracellular glycoprotein, fibronectin, accompanies condensation in both the developing limb and *in vitro* [2,3,6]. This altered matrix binds to cell-surface macromolecules such as integrins and heparan sulfate proteoglycan, causing their local accumulation in regions high in fibronectin [2,3]. The accumulated cells transiently epithelialize, *i.e.*, they form direct membrane to membrane contacts mediated by the appearance of the cell-cell adhesion molecules N-cadherin [7] and N-CAM [8]. Binding of fibronectin to integrins on the cell surface can also promote N-cadherin-mediated cell-cell adhesion [9]. Cellular automaton models of myxobacteria by Stevens and coworkers have explored the related problem of bacterial cell condensation and motion in the presence of chemotaxis and adhesion to a non-diffusing cell-secreted extracellular material [10–12] and also in the case of purely local interactions [13].

The CPM [14,15] provides a convenient way of simulating cell-cell interactions with non-uniform adhesion and cell-ECM interactions with non-uniform ECM distributions.

2 The 2D CPM Simulation

The 2D CPM represents the spatial distribution of a set of N cells, indexed by σ, by superimposing a lattice on the cells. The index value at a lattice site (i,j) is σ if the site lies in cell σ. Each cell occupies multiple lattice sites. We assign different surface energies between different cells according to their surface adhesiveness, which we denote by J. Smaller values of J correspond to stronger cell-cell adhesion. Cell shape changes correspond to deformation of the domains by changes of index at randomly selected sites. Evolution is Monte-Carlo-Boltzmann, using Metropolis dynamics. Cells rearrange diffusively to minimize the total effective free energy (see [14,15] for details).

We create a 600 × 600-pixel square lattice and restrict the initial cell distribution to a circle in the middle with diameter 600 pixels to represent the experimental diameter of 3 mm, setting the length scale to 5 μm/pixel. The typical limb bud mesenchymal cell is 15 μm in diameter, so cells have an area of approximately 7 pixels. The plating density is 1.75×10^7 cells/ml in a 10 μl spot. We assume an equivalent 2D density of about 40% spatial occupation. This ratio, which the spatial constraints on our 2D model dictate, is lower than the standard density in micromass cultures where cells are initially confluent and become separated by small amounts of secreted ECM before condensing [5]. In the limb bud the volume ratio of cells to ECM is about 3 to 2 [16].

In line with an earlier proposal [2,3] we implement a stochastic model for mesenchymal condensation which invokes only experimentally verified effects and components: mesenchymal cells in culture produce non-diffusing

fibronectin and deposit it onto the substrate. In our model fibronectin accumulates at the deposition site and does not decay or diffuse. Cells execute random walks biased by their binding more strongly to fibronectin than to the substrate. Fibronectin–cell-surface binding upregulates production of cell-cell adhesion molecules such as N-cadherin. The properties of the cells change during the experiment. The potential rate of fibronectin production increases five-fold 6 hours after plating (Fig. 1 (A)). We assign to each cell an initial random phase parameter. Each cell goes through a 24-hour cycle, potentially producing fibronectin during half of the period (Fig. 1 (C)). The actual fibronectin production is the product of Fig. 1 (A) and Fig. 1 (C). Statistically, at any time, half of the cell population is producing fibronectin. N-cadherin appears after 12 hours, increasing in proportion to the cell's integrated exposure to fibronectin, which we represent by decreasing the cell-cell interaction energy, J, linearly with the amount of fibronectin the cell has seen (Fig. 1 (B)). Condensations appear after 18 hours and continue expanding until 36 hours.

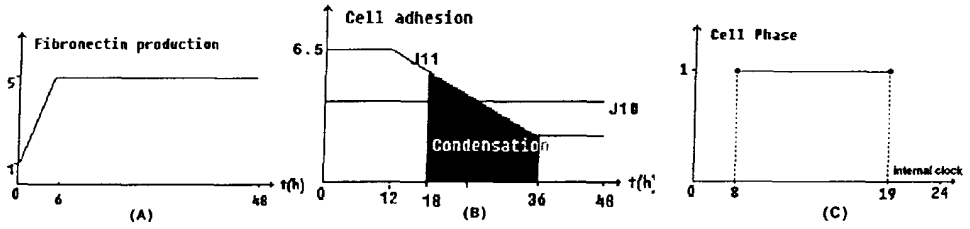

Fig. 1. (A) The potential fibronectin production of each cell. (B) The dependence of each cell's adhesiveness on the amount of fibronectin it has contacted. Shading shows the period of condensation. (C) The fibronectin production phase of a sample cell.

The Hamiltonian describes the interactions between cells and between cells and their environment. Our Hamiltonian includes three terms:

$$\mathcal{H} = \sum_{(i,j),(i',j')} J(\sigma,\sigma')(1-\delta_{\sigma(i,j),\sigma'(i',j')}) + \sum_{\sigma} \lambda(A_\sigma - A_{\text{Target},\sigma})^2 + \sum_{(i,j)} \mu C_f(i,j). \tag{1}$$

The first term describes the surface adhesion energy between cells and between cells and the ECM. The sum is over (i,j) and (i',j') neighbors, where only boundary pixels contribute. We use the 20, 4th nearest neighbors (pixels (i',j')) to pixel (i,j). τ is the cell type. We treat the environment, including the culture solution and substrate as a single cell with $\tau = 0$, while all the biological cells are of type $\tau = 1$. We denote the energy cost per unit area of cell surface between a cell σ and a cell σ' of type τ' by $J(\sigma,\tau')$. If $J(\sigma,\tau') \neq J(\sigma',\tau)$ we set the interaction energy per unit area between the cells to $J(\sigma,\sigma') = \min(J(\sigma,\tau'), J(\sigma',\tau))$. We make each cell's surface energy a variable to reflect the increase in membrane-bound adhesion molecules in response to fibronectin. The second term constrains the cell surface area and the sum is over all cells. λ is the compressibility of the cell (larger λ corre-

sponds to less compressible cells). A_σ is the actual cell area and $A_{\text{Target},\sigma}$ is the area of the cell in the absence of compression. The third term describes the effect of preferential attachment of cells to fibronectin and the sum includes only sites that lie within cells. $C_f(i,j)$ is the concentration of fibronectin at lattice site (i,j). μ is the unit strength of the fibronectin binding.

At each step we select a lattice site (i,j) at random and change its index from σ to σ' (where σ' is the index of a neighboring lattice site) with Boltzmann probability; for a temperature $T > 0$, $P(\sigma(i,j) \rightarrow \sigma'(i,j)) = \{\exp(-\Delta\mathcal{H}/kT)\text{: } \Delta\mathcal{H} > 0; 1\text{: } \Delta\mathcal{H} \leq 0\}$, where $\Delta\mathcal{H}$ is the energy gain in Eqn. 1 produced by the change. Each such move corresponds to cell σ' displacing cell σ by one lattice site. T is a fluctuation temperature corresponding to the amplitude of cytoskeletally driven cell membrane fluctuations. For more details on the CPM see [15,17,18].

3 Major Results

Patterns of mesenchymal condensation and resulting cartilage nodule formation at high (superconfluent) and low (confluent) culture density (Fig. 2) show very different morphologies.

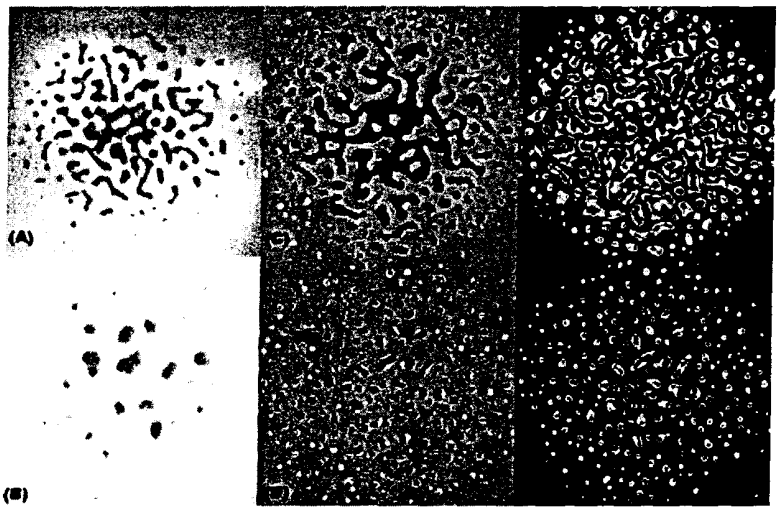

Fig. 2. Experimental images of Alcian blue-stained cartilage nodules that formed in cultures plated at superconfluent (A) and confluent (B) densities. The white background represents cells that failed to undergo condensation and therefore did not progress to cartilage. Unlike living cells in high density cultures, cells in our 2D simulations cannot readily move past one another. We therefore performed the simulations at subconfluent densities of 40% and 20% coverage. Similar to the experiment, the simulated cells form stripes and spots at high density (C) and only spots at low density (D). Simulated cells are initially white and become dark when the local fibronectin concentration exceeds a threshold chosen to correspond to Alcian blue staining. (E), (F) The distribution of fibronectin: the lighter-colored fibronectin peaks co-localize with the cell clusters.

When the density is relatively high (40%), the condensation consists of both spots and 'finger-like' stripes, while dots form in low density condensation (< 20%).

4 Discussion

μ represents the strength of cell-ECM binding, the smaller μ, the coarser the pattern. The stronger the upregulation of expression of cell adhesion molecules, the smaller the final J between cells and the coarser the pattern. In the range of parameters we tested, the period of the phase parameter is not crucial as long as cells alternate between a fibronectin producing phase and a non-producing phase [19,20]. The clustering is robust: the same pattern types occur over broad ranges of parameters.

Experimental studies of high density micromass cultures [21–23] have indicated, in line with earlier suggestions [5] that the pattern of condensations in high density micromass cultures is determined by a mechanism that employs both locally-acting cell-cell and cell-ECM adhesion mechanisms as well as globally-acting diffusible activators and inhibitors of ECM production, in Turing-type reaction-diffusion. The spot and stripe patterns seen in our simulations result from a density dependent mechanism that operates in the absence of diffusible activators and inhibitors. In our model, the instability arises from positive feedback: cells tend to stay longer in regions with fibronectin, and hence become more adhesive and produce more fibronectin. The wavelength grows continuously until cells become stuck and clusters cannot coalesce any more. Thus, unlike the Turing mechanism, where the diffusion constants of the activator and inhibitor determine the pattern wavelength, our mechanism has no intrinsic wavelength but coarsens. The duration and rate of coarsening together determine the final wavelength. High densities of cells lower the cells' motility and lead to more 'stripe-like' patterns while at low densities, cells move fast enough for the surface-energy driven rounding of clusters to dominate. Even for patterns of the same type, changes in parameter values result in subtle differences in cluster shape (Fig. 3).

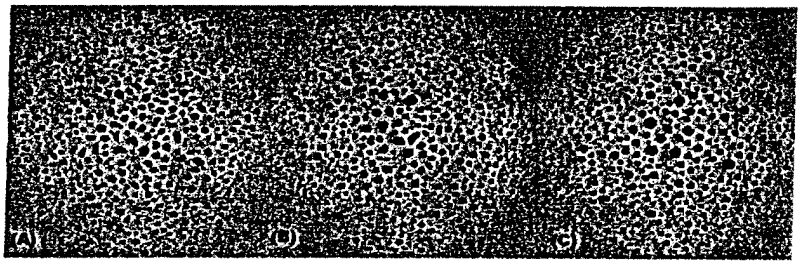

Fig. 3. Low density condensation. (A) $J_{cell-cell} = 4.5$. (B) $J_{cell-cell} = 2.5$ (C) $J_{cell-cell} = 0.5$. Larger Js result in faster sticking. The rate of surface tension driven rounding *vs.* the time to stick determines whether spots are round or rough and irregular, elongated or symmetrical, large or small.

We can test the applicability of our mesenchymal pattern formation mechanism in the *in vitro* setting by detailed statistical comparison of the distribution of condensations and the resulting nodules at a wide range of initial plating densities. Our preliminary results suggest that it will account for results at lower density better than those at higher density or in the limb bud itself, where evidence for lateral inhibition of incipient condensations is strong [24].

Appendix

Cell culture: We obtained fertile White Leghorn eggs from Avian Services, Inc. (Frenchtown, NJ). We prepared primary cultures by separately pooling dissociated mesenchymal cells from the myoblast-free distal 0.3 mm [25,26] of stage 24 [27] leg buds. [19] gives experimental details. The present study used lower plating densities: 2.0×10^5 (or 1.5×10^5 for dilution experiments) cells per 10 μl spot. We fixed sample cultures after six days of incubation and stained them for cartilage matrix with Alcian blue at pH 1.0 [28].

Acknowledgements Grants NSF-IBN-008365 and CAPES-Brazil. We thank Mark Alber and Cornelis Weijer for critical reading and discussion.

References

1. Newman, S. A.. *Trends Genet.* **4**, 329–332, 1988.
2. Frenz, D. A., Akiyama, S. K., Paulsen, D. F. and Newman, S. A.. *Dev. Biol.* **136**, 87–96, 1989.
3. Frenz, D. A., Jaikaria, N. S. and Newman, S. A.. *Dev. Biol.* **136**, 97–103, 1989.
4. Hall, B. K. and Miyake, T.. *Int. J. Dev. Biol.* **39**, 881–893, 1995.
5. Newman, S. A. and Tomasek, J. J.. *Extracellular Matrix*, Vol.2, Molecular Components and Interactions, Edited by Comper, W. D., 1996.
6. Tomasek, J. J., Mazurkiewicz, J. E. and Newman, S. A.. *Dev. Biol.* **90**, 118–126, 1982.
7. Oberlender, S. A. and Tuan, R. S.. *Development* **120**, 177–187, 1994.
8. Widelitz, R. B., Jiang, T. X., Murray, B. A. and Chuong, C. M.. *J. Cell Physiol.* **156**, 399–411, 1993.
9. Dufour, S., Beauvais-Jouneau, A., Delouvee, A. and Thiery, J. P.. *J. Cell Biol.* **146**, 501–516, 1999.
10. Stevens, A.. *Mathematical modeling and simulations of the aggregation of myxobacteria. Chemotaxis-equations as limit dynamics of moderately interacting stochastic processes.* Ph.D. Dissertation, Universität Heidelberg, 1992.
11. Othmer, H. G. and Stevens, A.. *SIAM J. Appl. Math.* **57**, 1044–1081, 1997.
12. Stevens, A.. *SIAM J. Appl. Math.* **61**, 172–182, 2000.
13. Lutscher, F. and Stevens, A.. *J. Nonlinear Science* **12**, 619–640, 2002.
14. Graner, F. and Glazier, J. A.. *Phys. Rev. Lett.* **69**, 2013–2016, 1992.
15. Glazier, J. A. and Graner, F.. *Phys. Rev. E* **47**, 2128–2154,1993.
16. Gould, R. P., Day, A. and Wolpert, L.. *Exp. Cell Res.* **72**, 325–336, 1972.

17. Jiang Y., Levine, H. and Glazier, J. A.. *Biophysical J.* **75**, 2615–2625, 1998.
18. Upadhyaya, A.. *Thermodynamic and Fluid properties of Cells, Tissues and Membranes.* Ph.D. Dissertation, University of Notre Dame, 2000.
19. Leonard, C. M., Fuld, H. M., Frenz, D. A., Downie, S. A., Massague, J. and Newman, S. A.. *Dev. Biol.* **45**, 99–109, 1991.
20. Ohsugi, K., Gardiner, D. M. and Bryant, S. V.. *Dev. Biol.* **189**, 13–21, 1997.
21. Miura, T. and Shiota, K.. *Anat. Record* **258**, 100–107, 2000.
22. Miura, T., Komori, M. and Shiota, K.. *Anat. Embryol. (Berl)* **201**, 419–28, 2000.
23. Miura, T. and Shiota, K.. *Anat. Rec.* **258**, 100–107, 2000.
24. Moftah, M. Z., Downie, S. A., Bronstein, N. B., Mezentseva, N., Pu, J., Maher, P. A. and Newman, S. A.. *Develop. Biol.* **249**, 270–282, 2002.
25. Brand, B., Christ, B. and Jacob, H. J.. *Am. J. Anat.* **173**, 321–340, 1985.
26. Newman, S. A., Pautou, M.-P. and Kieny, M.. *Dev. Biol.* **84**, 440–448, 1981.
27. Hamburger, V. and Hamilton, H. L.. *J. Morphol.* **88**, 49–92, 1951.
28. Downie, S. A. and Newman, S. A.. *Dev. Biol.* **162**, 195–208, 1994.